Multiferroic and magnetoelectric properties of BiFeO3-CoFe2O4-poly(vinylidene-flouride) composite films

Multiferroic and magnetoelectric properties of $BiFeO_3$-$CoFe_2O_4$-poly(vinylidene-flouride) composite films

Nidhi Adhlakha[1], K.L.Yadav[2], Marco Truccato[1], Manjusha[2], Piu Rajak[3], Alfio Battiato[1], Ettore Vittone[1]

[1]*Elettra-Sincrotrone Trieste S.C.p.A, Area Science Park, I-34012 Trieste, Italy.*
[2]*Smart Materials Research Laboratory, Department of Physics, Indian Institute of Technology Roorkee, Roorkee- 247667, India.*
[3]*Department of Metallurgical and Materials Engineering, Indian Institute of Technology (IIT) Madras, Chennai 600036, India*

*Corresponding Author: Tel.: +91 1332 285744; Fax: + 91 1332 273560
E-mail: klyadav35@yahoo.com

Abstract

Multiferroic thick nanocomposite films of (1-*x*)($0.3CoFe_2O_4$-$0.7BiFeO_3$)-*x*Polyvinylidene difluoride (CFO-BFO/PVDF) with *x* variations 0.20, 0.30 and 0.40 were synthesized using hot press method. Detailed measurements of structural, dielectric, magnetic and magnetoelectric data have been reported. Structural characterization reveals the presence of all the three distinct phases viz. CFO, BFO and PVDF. The dielectric loss as low as 0.05 has been observed for composite film with 40 mol% of PVDF. The AC conductivity (5.9×10^{-8} $ohm^{-1}cm^{-1}$) of composite film (*x*=0.40) is found to be much lower as compared to CFO-BFO ceramic. The electric poling of composite film (with *x*=0.30) leads to substantial increase in saturation ($2M_s$) and remnant magnetization ($2M_r$). A significant magnetoelectric effect with magnetoelectric voltage coefficient (α_{ME}) ~22.128 mV/cm Oe has been observed for composite film with *x*=0.40, which is possibly a consequence of implicit mechanical interaction between CFO and BFO through PVDF matrix. Hence these nanocomposite films hold a great potential to be promising candidates for multiferroic devices.

Keywords: Composite Films; Magnetoelectric Effect; Dielectric Response; Magnetic Measurements; Microstructure.

1. Introduction

Magnetoelectric multiferroics are considered to be promising materials both scientifically and technologically, and have been widely investigated over the last few decades [1-3]. These materials are characterized by the coupling between electronic and magnetic degrees of matter, where a change of electric polarization has been observed on application of magnetic field, and vice versa. This coupling can arise intrinsically, or extrinsically, mediated by elastic coupling between magnetostrictive and piezoelectric phases [4, 5]. These materials are potential candidates for multiple memory state elements, high density storage and spintronics [3, 6]. The single phase ME materials are intrinsically ME materials which show a small ME coupling at low temperatures, a restriction for their use in technological applications. Amongst the widely investigated multiferroic materials, $BiFeO_3$ (BFO) based single-phase systems have attracted the maximum attention owing to its multiferroic properties at room temperature. Indeed, BFO is antiferromagnetic below T_N ~ 653 K and ferroelectric below T_c ~ 1103 K, having a rhombohedrally distorted perovskite structure corresponding to *R3c* with G-type antiferromagnetic behavior [7, 8]. The emergence of BFO as a leading multiferroic candidate arises due to its high remnant polarization (~ 90 μC/cm^2) and magnetization (~1.0 Bohr magneton per unit cell) found in the thin films, which are much higher than that of bulk [9].

For devices based on magnetoelectric (ME) effect, in addition to good ferroelectric behavior a large magnetic moment is required [8]. However, BFO suffers from crucial problems such as low resistivity which is related to high leakage current density due to Bi ions volatility. In addition, it has antiferromagnetic ordering with weak magnetization. In spite of the fact that in the (111) plane Fe ions are in ferromagnetic ordering, there is a canted antiferromagnetic ordering between the neighbouring planes, resulting in cancellation of net magnetization in bulk [10]. These problems along with high dielectric loss create a hindrance to the use of BFO in fabrication of multifunctional devices. Numerous investigations based on possibility to tune the multiferroic properties of BFO through chemical substitution at A and B sites have been performed. Amongst them, the partial substitution of A site by Sm^{3+} [11, 12], Ho^{3+} [13], Nd^{3+} [14], and by replacing Fe atom with transition metal ions Sc^{3+} [15], Ti^{4+} [16], Mn^{4+} [17] etc. has been carried out. As a consequence, either ferroelectric or magnetic behavior has been improved. The substitution of Bi by rare-earth atom makes it possible to reduce the leakage current, whereas a relatively enhanced magnetization has been observed in the system having Fe substituted with transition metal ions. However, this enhancement is restricted as it can only suppress or destroy the spin cycloid, but cannot change the intrinsic anti-ferroelectric nature of BFO-based single-phase materials [18]. The magnitude of ME coupling observed in most of these materials at room temperature is insufficient for most of the proposed

applications. Therefore a new approach is needed to get useful values. In order to improve the magnetism of BFO, an effective way is to introduce $CoFe_2O_4$ (CFO) into BFO by forming its nanocomposite. CFO is a hard magnetic material having large saturation magnetization (about 80 emu/g) and high coercivity (5400 Oe), and is known for its large magnetostrictive coefficient, so it is used widely as piezomagnetic constituent [19]. The nanocomposite *x*CFO-(1-*x*)BFO with *x*=0.30 as reported by Liu et al. [20] is found to exhibit the largest coercivity and optimal squareness (remnant magnetization (M_r)/saturation magnetization (M_s)). It has also been reported recently that the antiferromagnetic nature of BFO in bulk can be transformed to weak ferromagnetic at nanoscale particle size, owing to suppressed spin spiral periodicity [21].

On the other hand, magnetoelectric composites exhibit an extrinsic ME effect, where a dimensional change is induced by magnetic field applying on magnetostrictive material, which is transferred to the adjacent piezoelectric material, further undergoes a mechanically induced change in its polarization. This ME product property leads to an output signal which is many orders of magnitude higher as compared to single-phase materials at room temperature. This property makes these materials attractive for device applications [22]. These composite materials can be of ceramic- or polymer- based. Despite that the ceramic-based ME materials have ME coefficient three orders of magnitude higher as compared to polymer-based ones, they are limited by undesirable reactions at the interface region, and may become fragile. This further leads to high dielectric losses, low electrical resistivity, which hinders their utility in device applications [23]. Nowadays polymer-based ME materials have attracted a huge attention due to their low processing temperature, cheap and facile production methods, and possess flexible structures such as thin sheets or molded shapes without large leakage currents [24]. Moreover, in polymer based materials due to direct contact of magnetostrictive material with the surrounding piezoelectric polymer matrix the strain coupling does not deteriorate with operation [25]. The use of polymer based composites is one of the ways to obtain high ME coupling, and to avoid the problems of leakage current and high dielectric breakdown strength associated with the ceramics.

Among a small class of polymers showing piezo-, pyro- and ferroelectricity, Poly(vinylidene fluoride) (PVDF) and copolymers exhibit the best electroactive performance, hence is a choice from application point of view [26]. Most of the interesting properties of PVDF are related to the strong electric dipole moment of its monomer unit, which is further attributed to electronegativity of fluorine atoms with respect to carbon and hydrogen atom. Therefore the dipole moment is associated with each polymer chain, perpendicular to the polymer chain [27]. Among the four crystal modifications associated with PVDF known as α, β, γ and δ; β and γ are the most electro-active ones. Here, the β-phase is the one with highest dipolar moment per unit cell (8×10^{-30} C m).as

compared to the other phases. Due to these qualities they are used in various applications such as sensors and transducers [28].

The elastic energy density is an important parameter to measure both stress and strain generation capability of PVDF material. When a polymer is strained the stored elastic energy density U_s is given by $U_s = \frac{1}{2}YS^2$, where Y is Young's modulus and S is strain. The total elastic energy density obtained from all the generated strains cannot exceed the input electric energy density, as the energy must be conserved. The input electric energy density for a linear dielectric material is $U_E = \frac{1}{2}K\varepsilon_0 E^2$, where E is the applied field, ε_0 is vacuum dielectric permittivity and K is dielectric constant of polymer. Hence for polymers with low dielectric constant high electric field is required to generate high input electric energy density which can be converted into strain energy, and vice versa [29]. The high permittivity and high electrostriction exhibited by PVDF as compared to other polymers makes it a potential candidate to achieve high field-induced strain. Hence we chose PVDF matrix which serve as stress transfer medium between piezoelectric and magnetic phases of ME composites

These CFO-BFO nanocomposites prepared by sol-gel method were embedded in PVDF polymer matrix which makes these polymer-hosted nanocomposites suitable for device applications, because of their high elasticity and high breakdown strength. In these polymer based nanocomposites, the problems of high leakage current and dielectric losses of BFO that generally lead to failure during operation can be eliminated [30]. Significantly, large ME coupling has been observed in this kind of polymer based nanocomposite films [22]. The polymer PVDF having high dielectric constant, acts as a matrix to improve the ME sensitivity of the composites, as PVDF matrix helps to transfer strain induced in magnetostrictive phase (CFO) to piezoelectric phase (BFO). PVDF exhibits the highest piezoelectric response among a class of polymers exhibiting piezoelectricity. As piezoelectricity is the fundamental requirement for ME response of the composites. However the piezoelectric response decreases with increasing the filler concentration which is attributed to the loss in flexibility of material, increased nanoparticle agglomerates and fragility of composite film [5, 31].

In the present work, we report the synthesis of (1-*x*)(0.3$CoFe_2O_4$-0.7$BiFeO_3$)- *x*Polyvinylidene difluoride (CFO-BFO/PVDF) (*x*=0.20, 0.30 and 0.40) nanocomposite films, exhibiting dielectric, magnetic, and magnetoelectric properties with low dielectric loss. These types of ME nanocomposite films combining the advantages of ceramics and polymers, require low processing temperature, which also ensures no chemical inter-diffusion of piezoelectric and magnetostrictive phases. Hence, they have become potential candidates for electronics industry due to their low cost and ease of preparation.

2. Experimental Method

2.1 Preparation of $CoFe_2O_4$-$BiFeO_3$ composite powder

Spinel-perovskite $x$$CoFe_2O_4$-(1-$x$)$BiFeO_3$ (x=0.30) composite was synthesized through sol gel process. The detailed procedure is reported elsewhere [19].

2.2 Composite film synthesis

To obtain (1-x)(0.3$CoFe_2O_4$-0.7$BiFeO_3$)-xPVDF (CFO-BFO/PVDF) nanocomposite films we mixed the CFO-BFO nanocomposites into PVDF polymer with various concentrations (20-40%) of PVDF by weight. The mixtures were ground for 6-7 h in an agate mortar. The mixture obtained was then pressed using a hot polymer press at 180 °C for 15 minutes under a pressure of ~20 MPa. The polymer composite films in the form of regular thin sheets having thickness ~ 0.14 mm were obtained after cooling down to room temperature. Conducting electrodes of silver having thickness ~ 0.5 mm and area ~ 2 × 2 mm^2 were deposited on both flat surfaces of films for electrical measurements. The phase identification of the synthesized materials was carried out using X-ray diffractometer (Bruker D8 Advance) at a scanning rate of 1°/min. at room temperature using CuKα radiation (λ=1.5418 Å). The surface morphology was analysed by taking Field Emission Scanning Electron Microscopy (FESEM) images with the help of FEI Quanta 200FEG electron microscope operating at an accelerating voltage of 20 kV. The dielectric measurements were carried out using an automated HIOKI 3532-50 Hi-Tester LCR meter. The magnetic measurements on composites were taken using Vibrating sample magnetometer (VSM) at room temperature in the range of -10 kOe ≤ H ≤ 10 kOe. The XPS measurements were performed in a ultrahigh vacuum (10^{-9} mbar) system equipped with-a VSW Class 100 Concentric Hemispherical Analyzer. The samples were mounted on a copper tape and analyzed using a non-monochromatic Al Kα (VSW TA10) x-ray source. Survey spectra energy step was fixed to 1 eV, while the energy step of the core lines spectra was set to 0.2 eV. The spectra were analysed and processed with the use of Unifit2008© software. Room temperature magnetoelectric voltage coefficients $\alpha_{ME} = dE/dH$ were measured under the variation of applied magnetic bias field using a lock in-amplifier after the electric poling of composite films.

3. Results and Discussion

3.1 Phase characterization and microstructural analysis

Figure 1 shows the X-ray diffraction patterns of hot pressed (1-x)(0.3CFO-0.7BFO)-xPVDF composite films with different concentrations of PVDF, along with the individual phases of 0.3CFO-0.7BFO and PVDF. The 0.3CFO-0.7BFO prepared through sol gel process exhibits mixed spinel–perovskite structure without any traces of impurities. All the peaks of 0.3CFO-0.7BFO can be identified for the separate phases perovskite (BFO) and

spinel (CFO), and comply with the reported values [32]. BFO crystallizes in a rhombohedrally distorted perovskite structure with space group *R3c*, and CFO has cubic spinel structure with space group *Fd-3m.* The XRD pattern of PVDF shows the existence of both crystalline and amorphous phases. The existence of mixed α- and β- phases is evident from the XRD graph of PVDF thick film. The intense and sharp peaks (marked as *) appearing at diffraction angles 2θ corresponding to 17.9° (100), 18.5° (020) and 26.7° (101) are attributed to α-PVDF, while the peak at 20° (110) corresponds to the presence of β- phase. The strong intensity of peak at 20° shows the predominance of β- phase in PVDF film [33]. The appearance of broad peak at around 2θ=12° for PVDF can be attributed to presence of amorphous polymer chain [34]. The XRD pattern of CFO-BFO/PVDF composite films clearly indicates the predominance of the sharp peaks corresponding to CFO-BFO (+). The intensities of peaks pertaining to PVDF (*) are not significant. This suppression is due to low concentration of PVDF matrix as compared to CFO-BFO filler. However as the percentage of polymer is increased we found some amorphousity (in terms of humps) which corresponds to the amorphous nature of PVDF.

There is an important issue regarding some contradictions in identification and quantification of both β- and γ-phases, which is due to similarity of β- and γ- phase specific conformations. Hence, Fourier Transformed Infrared Spectroscopy (FTIR) is required for the identifications of peaks very close to each other and provides valuable information about the structure of PVDF. Figure 2 shows the FTIR spectra of pure PVDF film and the corresponding band assignments are depicted in the Figure. α- phase can be easily detected due to presence of large number of characteristics bands corresponding to this phase like the absorption bands at 766, 795 and 976 cm^{-1}. The band at 840 cm^{-1} is common to both β- and γ- phases, but it has been recently accepted that this strong band only corresponds to the β- phase [27].

FTIR result is also useful to quantify the electroactive phase content of PVDF assuming that FTIR absorption follows the Lambert-Beer law. The relative fraction of the β- phase F(β) in the films can be calculated from two distinct absorption bands at 766 (α phase) and 840 cm-1 (β phase) by using the following equation [27]:

$$F(\beta) = \frac{A_\beta}{\left(\frac{K_\beta}{K_\alpha}\right) A_\alpha + A_\beta}$$

The absorption coefficients K_α and K_β at the respective wavenumbers of 766 and 840 cm-1 are calculated using Lambert-Beer law and their values are 6.1×10^4 and 7.7×10^4 cm^2mol^{-1} , respectively. A_α and A_β are the absorbance at 766 and 840 cm^{-1}.

Figure 3 shows the TEM image and Selected Area Diffraction (SAD) pattern of CFO-BFO nanocomposites used in the synthesis of the composite films. The average particle size is found to be ~ 15-20 nm, and they are crystalline in nature which is manifested from SAD pattern (inset of Figure 2).

FESEM micrographs of sintered CFO-BFO ceramic and CFO-BFO/PVDF composite films with different wt% of PVDF are shown in Figure 4 (a)-(d), respectively. The grain distribution of CFO-BFO ceramic (Fig. 3(a)) is not uniform: instead clusters of grains with large intergranular porosity are clear from the micrograph. It is clearly seen that in hot-pressed CFO-BFO/PVDF composites, (Fig. 4(b)-(d)) the CFO-BFO ceramic grains are well dispersed in the polymer matrix with small agglomeration. There is an even distribution of ceramic powder surrounded by PVDF matrix, indicating the 0-3 connectivity [32]. The bright grains corresponding to CFO-BFO ceramic are distributed in dark surface region of PVDF polymer matrix.

3.2 Dielectric behavior

3.2.1. Dielectric properties versus frequency

The frequency dependent variation of dielectric permittivity (ε_r) and dielectric loss (tanδ) were carried out for CFO-BFO ceramic and CFO-BFO/PVDF composite films at room temperature, and are shown in Figure 5 (a) and (b), respectively, over the range 1 kHz- 1MHz. The values of ε_r for all the samples decrease with increase of frequency. It is observed from the Figure that all the composite films exhibit high permittivity at lower frequency region, and with increase of frequency it decreases continuously. There is a strong dispersion of dielectric constant at low frequencies which merges at high frequencies. The material gets enough time to polarize at low frequencies, and due to less polarization time at higher frequencies dipoles donot get much time to align themselves in the field direction. In case of ME composites the electron exchange between coexisting Fe^{2+} and Fe^{3+} ions cannot follow the applied external electric field beyond a certain critical frequency, hence generally decreases monotonically with increasing frequency. However once the frequency is above 10 kHz, the entire dielectric behavior is dominated by the relaxation mechanism associated with copolymer phase [35].

The value of dielectric constant is found to decrease with increase of PVDF content. The possible reasons behind this decrease might be following: (i) Low value of dielectric constant of PVDF ~16, (ii) PVDF is well known for five different polymorphisms; of which the phases α, β, γ and δ are stable. It is confirmed on the basis of XRD studies (Figure 1) that PVDF is present in mixed phases of α and γ which are non-polar. Hence the contribution of electrical polarization is hindered due to non-polar nature of PVDF, and constrained polymer chain [36, 37]. The low frequency dispersion decrease with increase of PVDF content. The reason may be due to reduction of space charge effect, and low dielectric loss associated with PVDF [36].

The frequency dependence of dielectric loss of CFO-BFO/PVDF composite films with different percentage of PVDF is shown in Figure 5 (b). It shows a similar trend to that of dielectric constant. The observed values of dielectric losses are relatively low (< 0.5). There is marginal decrease of dielectric loss with increasing frequency. This may be ascribed to the fall in electrical conductivity with increase of frequency. Several factors contribute to the dielectric loss in composite films such as Debye loss factor, direct current conduction and MWS (Maxwell-Wagner-Sillars) polarization. The relatively high dielectric loss of composite film with x=0.30 as compared to other composite films may be ascribed to interfacial relaxation processes [38]. A small hike appears at low frequency region between 10 kHz to 100 kHz, which shows the activated space charge polarization at lower frequencies, and hence acts as a dipole. This also shows the presence of one more relaxation mechanism which arises due to coincidence of hopping frequency of charge carriers with external electric field [39].

3.2.2. Dielectric properties versus temperature

The temperature dependence of ε_r and tanδ at an applied frequency of 1 kHz for CFO-BFO/PVDF composite films is given in Figure 6 (a) and (b), respectively. The value of ε_r, which is a measure of polarization, increases continuously with increasing temperature up to a certain temperature. This can be described on the basis that dielectric response of ceramic-polymer composites can be considered as the contribution of all ionic, electronic and dipolar polarization of CFO-BFO ceramic, and dipolar orientational polarization of PVDF polymer. In addition, the segmental mobility of polymer increases with temperature, which facilitates the polarization of polar components, hence increases the dielectric constant [39].

However, there is no systematic variation of the temperature (T_{max}) corresponding to maximum ε_r. The value of dielectric constant is found to decrease with increase of PVDF content; at the same time dielectric loss also decreases. At room temperature the dielectric constant and dielectric loss decreases from ε_r ~ 227, tanδ ~ 0.122 to ε_r ~ 19.54, tanδ ~ 0.05 with increase of polymer content from 20 mol% to 40 mol%, respectively. This significant decrease of dielectric loss is attributed to the reduced electron tunneling in CFO-BFO ceramic in presence of polymer matrix, which further decreases the conduction loss [33].

3.2.3. AC conductivity

The AC conductivity (σ_{ac}) can be defined as $\sigma_{ac} = \omega\varepsilon_0\varepsilon_r tan\delta$, where ω is angular frequency and ε_0 is permittivity of vacuum. Figure 7(a) shows the variation of AC conductivity with temperature for all the composite films. The inset shows the AC conductivity of CFO-BFO ceramic. The σ_{ac} increases with increasing temperature. Actually conductivity due to non-stoichiometric oxygen vacancies is associated with BFO in whole

temperature range and at higher temperatures this effect becomes striking due to thermally activated process [40]. At room temperature the values of σ_{ac} were calculated to be 1.7×10^{-6}, 1.45×10^{-6}, 4.38×10^{-7} and 5.9×10^{-8} $\Omega^{-1}cm^{-1}$ for CFO-BFO ceramic, and composite films with x=0.20, 0.30 and 0.40, respectively. The σ_{ac} is found to decrease with polymer content, which might correspond to a decrease in the number of conduction paths between the grains due to the increasing presence of PVDF at the interface of BFO and CFO.

The temperature dependence of conductivity seems to follows the Arrhenius equation: $\sigma = \sigma_0 \exp\left(-\frac{E_a}{K_B T}\right)$, where σ_0 is pre-exponential factor, E_a is activation energy per charge carrier, K_B is Boltzmann's constant and T (K) is the absolute temperature. Indeed, experimental data could be roughly fitted by the typical Arrhenius law describing thermally activated conduction processes [41] as shown in Figure 7 (b). The corresponding activation energy obtained by the fits is included in Figure 7 (b).

3.3 Magnetic properties

Figure 8 shows the magnetization (M) versus applied field (H) of CFO-BFO ceramic (x=0) and CFO-BFO/PVDF composite films (x=0.20, 0.30 and 0.40) at room temperature. The magnetic parameters such as saturation magnetization (M_s), remnant magnetization (M_r) and coercivity (H_c) determined by the hysteresis loop measurements are given in Table 1. The magnetism observed in 0.3CFO-0.7BFO ceramic (x=0) is attributed to the combined effects of BFO and CFO as described in our previous study [19]. Although BFO exhibits weak magnetization of 0.15 emu/g at 75 kOe and is a canted antiferromagnet [42], however there is generation of spin disorder with reduction of particle size and spin spiral structure is broken [30]. As demonstrated by Park et al. [43], with decrease of particle size the magnetization of BFO increases. Moreover, it should be noted here that the strain existing in the grain boundaries between BFO and CFO might change the spin orientation of BFO grains in the composite [44]. The presence of an ordered magnetic structure is evident from the typical ferromagnetic behavior shown by the composite films. The M-H loop of pure CFO-BFO (x=0) is not completely saturated (even at 75 kOe), whereas the composite films (x=0.20, 0.30 and 0.40) exhibit fully saturated magnetic hysteresis loops at room temperature. The value of saturation magnetization (M_s) is found to decrease with increase of PVDF content as shown in inset of Figure 7. According to equation $M_s = \varphi m_s$; where φ is volume fraction of particles and m_s is saturation moment of a single particle, an increase of nonmagnetic PVDF is expected to induce a decrease of the volume fraction of ferrite particles and therefore a decrease of the total saturation magnetization. However, it can be observed from the inset of Figure 8 that the decrease of M_s is more than linear as a function of φ. A possible reason for this behaviour could be represented by the presence of a magnetic dead layer on the grain surface [45].

3.4 Magnetoelectric Properties

The magnetoelectric (ME) coupling in CFO-BFO/PVDF composite films at room temperature was demonstrated by measuring the effect of dc electric field poling on magnetic hysteresis loops. Two pieces of same polymer film (x=0.30) were taken, one of them was as- prepared (un-poled) and other was electrically poled at 30 kV/cm for 10 minutes. Figure 9 shows the M-H hysteresis loops of both un-poled and poled CFO-BFO/PVDF composite film with x=0.30. The magnetic parameters $2M_s$, $2M_r$ and $2H_c$ calculated from hysteresis loop obtained after poling are 22.506 emu/g, 9.571 emu/g and 1.855 kOe, respectively. There is a significant increase of both the saturation and remnant magnetization in the poled film. The drastic change in the behaviour of M-H curve revealed in poled composite film shows the presence of strong magnetoelectric coupling in the composite films. Similar results are reported by many other research groups [46-48]. The electric dipoles align along the direction of the applied electric field; due to interaction between CFO and BFO through PVDF matrix the motion of electric domains alters the local strain, resulting in change in magnetic anisotropy, and correspondingly increasing the magnetization [48].

The coupling between electric and magnetic dipole interactions at atomic level is confirmed by determining the ME coupling coefficient (using dynamic method) of the samples; $\alpha_{ME} = \frac{\delta E}{\delta H} = \frac{\delta V}{t\delta H}$, where E is electric field, H is magnetic field, and t is total thickness of the sample. Before taking ME measurements the samples were poled at an applied electric field of 1 kV/cm at 100 ˚C for 1 h. ME coupling arises mainly from magnetic-mechanical-electrical transform via stress mediated transfer in the interface [49]. The shape of magnetic particles (CFO) changes due to magnetostriction with the application of magnetic field and through the polymer matrix the strain produced is transferred to piezoelectric phase (BFO) which further gives rise to the induced changes.

Figure 10 (a)-(d) shows the magnetic field (H_{dc}) dependence of longitudinal (E parallel to H) ME voltage coefficient α_{ME} measured by superimposing an ac magnetic field of 3 Oe (f = 999Hz), with a sweeping DC magnetic field from 0-8000 Oe. H_{dc} corresponding to α maximum in our case does not match with the H_c obtained from hysteresis measurements. This implies that α_{ME} is related to magnetic field dependence of differential magnetostriction ($\frac{d\lambda}{dH}$) [50]. The value of α_{ME} of the samples increases, and at a particular value of H_{dc} it starts to decrease. This behavior is explained by increase of effective piezomagnetic coefficient until an appropriate dc magnetic field is reached. Further, with increasing the applied dc magnetic field, a decrease of induced voltage is observed which arises due to saturation of magnetostriction coefficient. Hence α_{ME} decreases at high value of magnetic field [51, 4]. Figure 10(e) shows the variation of α_{ME} at the maxima with polymer content in CFO-BFO. Pure CFO-BFO ceramics shows the ME coefficient of 1.420 mV/cm-Oe. The low value

of ME response in pure CFO-BFO ceramics is attributed to the presence of secondary phases and low resistivity due to Fe valence fluctuation. However, with the addition of polymer content, an improved ME response has been observed; since the CFO-BFO/PVDF composite films with x=0.20, 0.30 and 0.40 have α_{ME} =1.927, 5.785 and 22.128 mV/cm-Oe, respectively at the maxima. Some theoretical predictions of effective magnetoelectric coefficients of composites show that the maximum magnetoelectric performance is not obtained for the nanocomposite with largest piezoelectric coefficient. Similarly the low value of filler content (7 wt% of ferrite content) is not enough to provide higher magnetoelectric coupling. Since magnetoelectric effect is product property, hence a substantial presence of both the ferroelectric and magnetostrictive phases is necessary as the stiffness of both phases is comparable in magnitude, and elastic interaction is strongest [52, 53]. The maximum magnetoelectric effect induced and its variation with applied magnetic field in piezoelectric polymer based composites depends on several factors such as type of ferrite, weight percentage of ferrite content and magnetic field intensity and direction [54]. The induced ME coefficient is larger than observed for other ME composites [55-57].

3.5 XPS studies

XPS analysis was performed on 0.3CFO-0.7BFO ceramic and 0.8(0.3$CoFe_2O_4$-0.7$BiFeO_3$)-0.2PVDF composite film to identify the chemical bonding. Figure 11 (a) presents the wide range spectrum of 0.8(CFO-BFO)-0.2PVDF composite film. It is apparent that Fe2p peak is overwhelmed by F1s signal; this fact suggests that CFO-BFO particles are embedded in the PVDF matrix deeper than the XPS probing depth, which is smaller than 10 nm [39]. This interpretation is corroborated by Fig. 11 (b) which shows a comparison of detailed XPS spectra of the Fe and F core levels, derived from 0.3CFO-0.7BFO ceramic and 0.8(CFO-BFO)-0.2PVDF composite film; the former shows the Fe 2p3/2 and Fe 2p1/2, which are absent in the CFO-BFO-PVDF spectrum. In order to further clarify the oxidation of Fe, Figure 11 (b) shows the Fe 2p XPS spectra of 0.3CFO-0.7BFO ceramic and 0.8(CFO-BFO)-0.2PVDF composite film. The core level binding energies were aligned with respect to C1s peak (285 eV) [58]. We also tried to perform the XPS analysis after scratching the polymer surface but the strong signal of fluorine is always present which covers the weak signal coming from Fe.

4. Conclusions

Summarizing, we have demonstrated the three phase nanocomposite films synthesized by embedding CFO-BFO ceramic in PVDF matrix by hot press method. Microstructural characterization reveals the CFO-BFO ceramic dispersed in PVDF polymer matrix. The nanocomposite film (with x=0.40) exhibits significantly low dielectric loss (~0.05) and low ac conductivity (order of 5.9×10^{-8} $ohm^{-1}cm^{-1}$) compared to bulk CFO-BFO. The magnetic

hysteresis loops observed at room temperature shows the decrease of total magnetization with increase of nonmagnetic PVDF. The electric control of magnetization is suggested by increase of magnetization on poling the composite film with electric field which is further attributed to reorientation of the spins. A strong room temperature ME coupling is exhibited by the composite films with ME coupling coefficient increasing with vol% of PVDF. The ME coupling of the particulate composite films improves significantly due to improved displacement transfer capability of flexible PVDF matrix. The results indicate the composite films as attractive candidates for memory storage and spintronic devices.

ACKNOWLEDGEMENT

This work has been partly carried out under project NANO-X jointly approved and funded by University of Torino and Compagnia di San Paolo. One of the authors (Nidhi Adhlakha) acknowledges support by the Abdus Salam International Centre for Theoretical Physics, Trieste, Italy, under the ICTP-TRIL fellowship scheme.

References

[1] C.W. Nan, M.I. Bichurin, S. Song, D .Viehland, G. Srinivasan, Multiferroic magnetoelectric composites: Historical perspective, status, and future directions, J. Appl. Phys. 103 (2008) 031101-031135.

[2] W. Eerenstein, N.D. Mathur, J.F. Scott, Multiferroic and magnetoelectric materials, Nature 442 (2006) 759-765.

[3] Z. Shi, C. Wang, X. Liu, C. Nan, A four-state memory cell based on magnetoelectric composite, Chin. Sci. Bull. 53 (2008) 2135-2138.

[4] P. Martins, Y.V. Kolensko, J. Rivas, and S. L. Medez, Tailored Magnetic and Magnetoelectric Responses of Polymer-Based Composites, ACS Appl. Mater. Interfaces 7 (2015) 15017-15022.

[5] P. Martins, A. Larrea, R. Gonçalves, G. Botelho, E. V. Ramana, S. K. Mendiratta, V. Sebastian, and S. Lanceros-Mendez, Novel Anisotropic Magnetoelectric Effect on δ-FeO(OH)/P(VDF-TrFE) Multiferroic Composites, ACS Appl. Mater. Interfaces 7 (2015) 11224−11229.

[6] M. Fiebig, T. Lottermoser, D. Frohlich, A.V. Golsev, R.V. Pisarev, Observation of coupled magnetic and electric domains, Nature 419 (2002) 818-820.

[7] G. Catalan, J.F. Scott, Physics and Applications of Bismuth Ferrite, Adv. Mater. 21 (2009) 2463-2485.

[8] I. Coondoo, N. Panwar, I. Bdikin, V.S. Puli, R.S. Katiyar, A.L. Kholkin, Structural, morphological and piezoresponse studies of Pr and Sc co-substituted $BiFeO_3$ ceramics, J. Phys. D: Appl. Phys. 45 (2012) 055302-055308.

[9] J. Wang, J.B. Neaton, H. Zheng, V. Nagarajan, S.B. Ogae, B. Liu, D. Viehland, V. Vaithyanathan, D.G. Scholm, U.V. Waghmare, N.A. Spaldin, K.M. Rabe, M. Wuttig, R. Ramesh. Epitaxial $BiFeO_3$ Multiferroic Thin Film Heterostructures. Science 299 (2003)1719-1722.

[10] J.S. Hwang, J.Y. Cho, S.Y. Park, Y.J. Yoo, P.S. Yoo, B.W. Lee, Y.P. Lee, Multiferroic properties of Stretchable $BiFeO_3$ nano-composite films, Appl. Phys. Lett. 106 (2015) 062902-062906.

[11] V.A. Khomchenko, J.A. Paixao, V.V. Shvartsman, P. Borisov, W. Kleemann, D.V. Karpinsky, A.L. Kholkin, Effect of Sm substitution on ferroelectric and magnetic properties of $BiFeO_3$. Scr. Mater. 62 (2010) 238-241.

[12] V.A. Khomchenko, J.A. Paixao, B.F.O. Costa, D.V. Karpinsky, A.L. Kholkin, I.O. Troyanchuk, V.V. Shvartsman, P. Borisov, W. Kleeman, Structural, ferroelectric and magnetic properties of $Bi_{0.85}Sm_{0.15}FeO_3$ Perovskite, Cryst. Res. Techn. 46 (2011) 238-242.

[13] Q. Xu, H. Zai, D. Wu, T. Qiu, M.X. Xu, The magnetic properties of $Bi(Fe_{0.95}Co_{0.05})O_3$ ceramics. Appl.

Phys. Lett. 95 (2009) 112510-112512.

[14] R.K. Mishra, D.K. Pradhan, R.N.P. Choudhary, A. Banerjee, Dipolar and magnetic ordering in Nd-modified $BiFeO_3$ nanoceramics. J. Magn. Magn. Mater. 320 (2008) 2602-2607.

[15] S.R. Shannigrahi, A. Huang, N. Chandrasekhar, D. Tripathy, A.O. Adeyeye, Sc modified multiferroic $BiFeO_3$ thin films prepared through a sol-gel process, Appl. Phys. Lett. 90 (2007) (022901-022903.

[16] L. Hongri, S. Yuxia, Substantially enhanced ferroelectricity in Ti doped $BiFeO_3$ films, J. Phys. D: Appl. Phys. 40 (2007) 7530-7533.

[17] M. Azuma, H. Kanda, A.A. Belik, Y. Shimakawa, M. Takano, Magnetic and structural properties of $BiFe_{1-x}Mn_xO_3$, J. Magn. Magn. Mater. 310 (2007)1177-1179.

[18] H. Yang, Q. Ke, H. Si , J. Chen, $0.7BiFeO_3$-$0.3BaTiO_3$-$Y_3Fe_5O_{12}$ composites with simultaneously improved electrical and magnetic properties, J. Appl. Phys. 2012; 111(2):024104-024107.

[19] N. Adhlakha, K.L. Yadav, Ripandeep Singh, Effect of $BaTiO_3$ addition on structural, multiferroic and magneto-dielectric properties of $0.3CoFe_2O_4$–$0.7BiFeO_3$ ceramics, Smart Mater. Struct. 23 (20140 105024-105039.

[20] X.M. Liu, S.Y. Fu, C.J. Huang, Synthesis and magnetic characterization of novel $CoFe_2O_4$–$BiFeO_3$ Nanocomposites, Mater. Sci. Eng. B 121 (2005) 255-260.

[21] S.M. Selbach, T. Tybell, M.A. Einarsrud, T. Grande, Size dependent properties of multiferroic $BiFeO_3$ Nanoparticles, Chem. Mater. 19 (2007) 6478-6484.

[22] P. Martins and S. L. Méndez, Polymer-Based Magnetoelectric Materials Adv. Funct. Mater. 23 (2013), 3371–3385.

[23] L. Mitoseriu, V. Buscaglia, M. Viviani, M.T. Buscaglia, I. Pallecchi, C. Harnagea, A. Testino, V. Trefiletti, P. Nanni, A.S. Siri, $BaTiO_3$–$(Ni_{0.5}Zn_{0.5})Fe_2O_4$ ceramic composites with ferroelectric and magnetic properties, J. Eur. Ceram. Soc. 27 (2007) 4379-4382.

[24] R. Gonçalves, A. Larrea, T. Zheng, M. J. Higgins, V. Sebastian, S. L. Mendez, P. Martins, Synthesis of highly magnetostrictive nanostructures and their application in a polymer-based magnetoelectric sensing device, Eur. Polym. J., 84 (2016) 685-692.

[25] R. Gonçalves, P. Martins, D. M. Correia V. Sencadas, J. L.Vilas, L. M. Leónc, G. Botelho, S. Lanceros-Méndez, Development of novel magnetoelectric $CoFe_2O_4$/poly(vinylidene fluoride) microspheres, RSC Adv.s 5 (45) (2015) 35852-35857.

[26] P. Martins, A. Lasheras, J. Gutierrez, J. M. Barandiaran, I. Orue and S. L. Mandez, Optimizing

piezoelectric and magnetoelectric responses on CoFe2O4/(P(VDF-TrFE) nanocomposites, J. Phys. D: Appl. Phys. 44 (2011) 495303-495309.

[27] P. Martins, A.C. Lopes, S. L. Mendez, Electroactive phases of poly(vinyledene fluoride): Determination, processing and applications, Progress in Polymer Science 39 (2014)683-706.

[28] R.P. Ummer, B. Raneesh, C. Thevenot, D. Rouxel, S. Thomas, N. Kalrikkal Electric, magnetic, Piezoelectric and magnetoelectric studies of phase pure ($BiFeO_3$-$NaNbO_3$)-(P(VFF-TrFE)) nanocomposite films prepared by spin coating, RSC Adv. 6 (2016) 28069-28080.

[29] Q.M. Zhang, H. Li, M. Poh, F. Xia, Z.Y. Cheng, H. Xu, C. Huang, An all-organic composite actuator material with a high dielectric constant, Nature 419 (2002) 284-287.

[30] A. Ahlawat, S. Satapathy, S. Bhartiya, M.K. Singh, R.J. Choudhary, P.K. Gupta, $BiFeO_3$/poly(methyl methacrylate) nanocomposite films: A study on magnetic and dielectric properties, Appl. Phys. Lett. 104 (2014) 042902-042906.

[31] P. Martins, D. Silva, M. P. Silva, and S. Lanceros-Mendez, Improved magnetodielectric coefficient on polymer based composites through enhanced indirect magnetoelectric coupling, Appl. Phys. Lett. 109, 112905 (2016).

[32] S.T. Zhang, L.Y. Ding, M.H. Lu, Z.L. Luo, Y.F. Chen, Preparation and multiferroic properties of $Bi_{0.8}La_{0.2}FeO_3$–$CoFe_2O_4$ ceramics, Solid State Commun. 148 (2008) 420-423.

[33] J. Rani, K.L. Yadav, S. Prakash, Structural and magnetodielectric properties of Poly(vinylidenefluoride)-[0.8($Bi_{0.5}Na_{0.5}$)TiO_3-0.2$CoFe_2O_4$] polymer composite films, Compos Part B-Eng. 79 (2015)138-143.

[34] M.S. Tamboli, P.K. Palei, S.S. Patil, M.V. Kulkarni, N.N. Maldar, B.B. Kale, Polymethyl methacrylate (PMMA)-bismuth ferrite (BFO) nanocomposite: low loss and high dielectric constant materials with Perceptible magnetic properties. Dalton Trans. 43 (2014) 13232-13241.

[35] X. Liu, S. Liu, M. G. Han, L. Zhao, H. Deng, J. Li, Y. Zhu, L. Krusin-Elbaum,and S. O'Brien Magnetoelectricity in $CoFe_2O_4$ nanocrystal-P(VDF-HFP) thin films, Nanoscale Res Lett. 8 (2013) 374.

[36] P. Thomas, K.T. Varughese, K. Dwarakanath, K.B.R.Varma, Dielectric properties of Poly(vinylidene fluoride)/$CaCu_3Ti_4O_{12}$ composites, Compos. Sci. Technol. 70 (2010) 539-545.

[37] P.K. Patel, K.L. Yadav, S. Dutta, Development of $Ba_{0.95}Sr_{0.05}(Fe_{0.5}Nb_{0.5})O_3$/poly(vinylidene-fluoride) nanocomposites for energy storage, J. Mater. Sci.: Mater. Electron. 26 (2015) 4165–4171.

[38] O.D. Jayakumar, E.H. Abdelhamid, V. Kotari, B.P. Mandal, R. Rao, Jagannath, V.M. Naik, R. Naik, A.K. Tyagi, Fabrication of flexible and self-standing inorganic–organic three phase magneto-dielectric PVDF

Based multiferroic nanocomposite films through a small loading of graphene oxide (GO) and Fe_3O_4 nanoparticles, Dalton Trans 44 (2015)15872-15881.

[39] T. Badapanda, V. Senthil, S. Anwar, L.S. Cavalcante, N.C. Batista, E. Longo, Structural and dielectric properties of polyvinyl alcohol/barium zirconium titanate polymer-ceramic composite, Curr. Appl. Phys. 13 (2013)1490-1495.

[40] S. Zhang, S. Priya, T.R. Shrout, C.A. Randall Low frequency polarization behavior of xBiScO$_3$-yBiGaO$_3$-(1-x-y)PbTiO$_3$ piezocrystals, J. Appl. Phys. 93 (2003) 2880-2883.

[41] Y. Saad, I.Á. Serrano, M.L. López, M. Hidouri, Structural and dielectric characterization of new lead-free perovskites in the ($SrTiO_3$)–($BiFeO_3$) system, Ceram. Int. 42 (2016) 8962-8973.

[42] N. Adhlakha, K.L. Yadav, R. Singh, Implications of La and Y codoping on structural, multiferroic, magnetoelectric and optical Properties of $BiFeO_3$,. Sci. Adv. Mater. 5 (2013) 947-959.

[43] T.J. Park, G.C. Papaefthymiou, A.J. Viescas, A.R. Moodenbaugh, S.S. Wong, Size-Dependent Magnetic Properties of Single-Crystalline Multiferroic $BiFeO_3$ Nanoparticles, Nano Lett. 7 (2007) 766-772.

[44] H.B. Sharma, K.N. Devi, V. Gupta, J.H. Lee, S.B. Singh, Ac electrical conductivity and magnetic properties of $BiFeO_3$–$CoFe_2O_4$ nanocomposites, J. Alloys Compd. 599 (2014) 32–39.

[45] A.A. Farghali, M. Moussa, M.H. Khedr, Synthesis and characterization of novel conductive and magnetic nano-composites, J. Alloys Compd. 499 (2010) 98–103.

[46] P. Ahuja, R. Sharma, C. Prakash, R.P. Tondon, Synthesis and characterization of $Ni_{0.8}Co_{0.2}Fe_2O_4$-$Ba_{0.95}Sr_{0.05}TiO_3$ multiferroic composites, Ceram. Int. 39 (2013) 9435-9445.

[47] R. Rani, J.K. Juneja, S. Singh, K.K. Raina, C. Prakash, Study of 0.1$Ni_{0.8}Zn_{0.2}Fe_2O_4$-0.9$Pb_{1-3x/2}La_xZr_{0.65}Ti_{0.35}O_3$ magnetoelectric composites, J. Magn. Magn. Mater. 325 (2013) 47-51.

[48] A. Singh, I. Choudhary, S. Mehta, S. Dahiya, C.S. Walia, K.K. Raina, R. Chatterjee, Optimal multiferroic properties and enhanced magnetoelectric coupling in $SmFeO_3$–$PbTiO_3$ solid solutions, J. Appl. Phys. 107 (2010) 084106-084109.

[49] V.S. Puli, A. Kumar, N. Panwar, I.C. Panwar, R.S. Katiyar, Transition metal modified bulk $BiFeO_3$ with improved magnetization and linear magneto-electric coupling, J. Alloys Compd. 509 (2011) 8223-8227.

[50] E.V. Ramana, A. Mahajan, M.P.F. Graca, A. Srinivas, M.A. Valente, Ferroelectric and magnetic properties of magnetoelectric $Na_{0.5}Bi_{0.5}TiO_3$-$BiFeO_3$ synthesized by acetic acid assisted sol-gel method, J. Eur. Ceram. Soc. 34 (2014) 4201-4211.

[51] K.C.Verma, J. Kaur, N.S. Negi, R.K. Kotnala, Multiferroic and magnetoelectric properties of

Nanostructures $BaFe_{0.01}Ti_{0.99}O_3$ thin films obtained under polyethylene glycol conditions. Solid State Comm. 178 (2014) 11-15.

[52] P. Martins, A. Lasheras, J. Gutierrez, J. M. Barandiaran, I. Orue and S. Lanceros-Mendez, Optimizing piezoelectric and magnetoelectric responses on $CoFe_2O_4$/P(VDF-TrFE) nanocomposites, J. Phys. D: Appl. Phys. 44 (2011) 495303.

[53] P. Martins, X. Moya, L. C. Phillips, S. Kar-Narayan, N. D. Mathur and S. Lanceros-Mendez, Linear Anhysteretic direct magnetoelectric effect in $Ni_{0.5}Zn_{0.5}Fe_2O_4$/poly(vinylidene fluoride-trifluoroethylene) 0-3 nanocomposites, Journal of Physics D: Applied Physics, 44 (2011) 482001-482004.

[54] T. Prabhakarana and J. Hemalatha, Magnetoelectric investigations on Poly (vinylidene fluoride)/$NiFe_2O_4$ flexible films fabricated through solution casting method, RSC.Adv. (2016) 1-7.

[55] R.V. Krishnaiah, A. Srinivas, S.V. Kamat, T. Karthik, S. Asthana, Effect of $CoFe_2O_4$ mole percentage on multiferroic and magnetoelectric properties of $Na_{0.5}Bi_{0.5}TiO_3/CoFe_2O_4$ particulate composites, Ceram. Int. 40 (2014) 7799-7804.

[56] C.M. Kanamadi, B.K. Das, C.W. Kim, D.I. Kang, H.G. Cha, E.S. Ji, A.P. Jadha, B.E. Jun, J.H. Jeong, B.C. Choi, B.K. Chougule, Y.S. Kang, Mater. Chem. Phys. 116 (2009) 6-10.

[57] R. Rani, J.K. Juneja, S. Singh, P. Chandra, K.K. Raina, Structural, electrical, magnetic and magnetoelectric properties of composites, J. Mag. Mag. Mater. 345 (2013) 55-59.

[58] http://srdata.nist.gov/xps/Default.aspx.

Table 1. Magnetic parameters of (1-*x*)($0.3CoFe_2O_4$-$0.7BiFeO_3$)-*x*PVDF composite films observed at 300 K.

Composition (*x*)	**$2M_r$ (emu g^{-1})**	**$2M_s$ (emu g^{-1})**	**$2H_c$ (kOe)**
0	11.536	32.8614	1.5606
0.20	11.210	22.0589	2.427
0.30	7.293	15.569	2.166
0.40	4.9012	10.740	2.249

Figure Captions

Figure 1. X-ray diffraction pattern for the (1-*x*)(0.3$CoFe_2O_4$-0.7$BiFeO_3$)-*x*PVDF composite films with *x*=0.20, 0.30 and 0.40 along with the individual phases viz. 0.3CFO-0.7BFO and PVDF.

Figure 2. FTIR spectrum of pure PVDF thick film.

Figure 3. TEM image of CFO-BFO ceramic, and the inset shows the corresponding Selected Area Diffraction (SAD) pattern.

Figure 4. FESEM micrographs of (a) sintered CFO-BFO ceramic and (1-*x*)(0.3$CoFe_2O_4$-0.7$BiFeO_3$)-*x*PVDF composite films with (b) *x*=0.20, (c) *x*=0.30, and (d) *x*=0.40, respectively.

Figure 5. (a) Dielectric constant (ε_r) and (b) tanδ versus frequency for (1-*x*)(0.3$CoFe_2O_4$-0.7$BiFeO_3$)-*x*PVDF composite films at room temperature.

Figure 6. Variation of (a) ε_r and (b) tanδ of (1-*x*)(0.3$CoFe_2O_4$-0.7$BiFeO_3$)-*x*PVDF composite films as a function of temperature at 1 kHz frequency.

Figure 7. (a) Thermal variation of ac conductivity (σ_{ac}) for (1-*x*)(0.3$CoFe_2O_4$-0.7$BiFeO_3$)-*x*PVDF composite films and (b) Corresponding variation of Log σ vs. T^{-1}. Solid lines represent the fitting using Arrhenius equation.

Figure 8. Magnetic hysteresis (M-H) loops of (1-*x*)(0.3$CoFe_2O_4$-0.7$BiFeO_3$)-*x*PVDF composite films at room temperature. Inset: Variation of M_s with concentration of PVDF (*x*)

Figure 9. Magnetic hysteresis loops of (1-*x*)(0.3$CoFe_2O_4$-0.7$BiFeO_3$)-*x*PVDF composite film with *x*=0.30; as prepared and after poling in dc electric field of 30 kV cm^{-1}.

Figure 10. Variation of α_{ME} with dc magnetic field of (1-*x*)(0.3$CoFe_2O_4$-0.7$BiFeO_3$)-*x*PVDF composite films with (a) *x*=0, (b) *x*=0.20, (c) *x*=0.30 and (d) *x*=0.40, respectively; (e) α_{ME} as function of composition (*x*).

Figure 11. (a) XPS wide range spectrum analysis for 0.8(CFO-BFO)-0.2PVDF composite film, (b) Fe 2p XPS spectra of CFO-BFO and 0.8(CFO-BFO)-0.2PVDF.

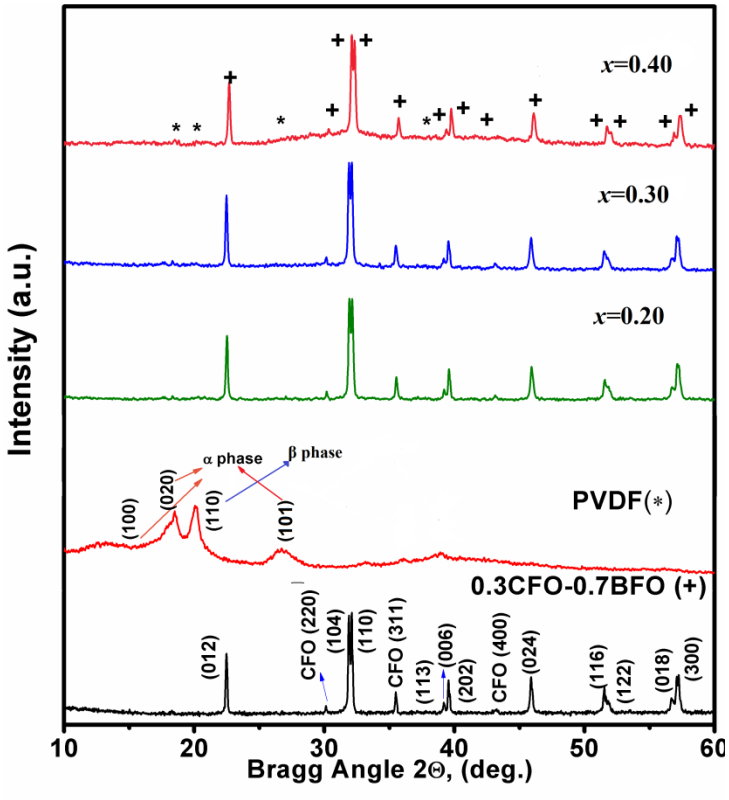
x=0.40
x=0.30
x=0.20
α phase
β phase
(100)
(020)
(110)
(101)
PVDF(∗)
0.3CFO-0.7BFO (+)
(012)
CFO (220)
(104)
(110)
CFO (311)
(113)
(006)
(202)
CFO (400)
(024)
(116)
(122)
(018)
(300)
Intensity (a.u.)
10
20
30
40
50
60
Bragg Angle 2Θ, (deg.)

Figure 1

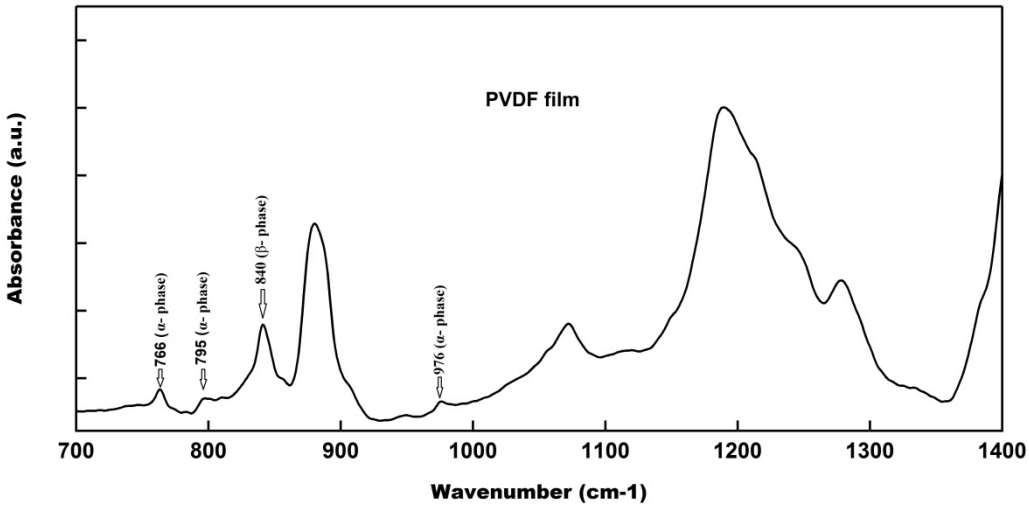
PVDF film
Absorbance (a.u.)
766 (α- phase)
795 (α- phase)
840 (β- phase)
976 (α- phase)
700
800
900
1000
1100
1200
1300
1400
Wavenumber (cm-1)

Figure 2

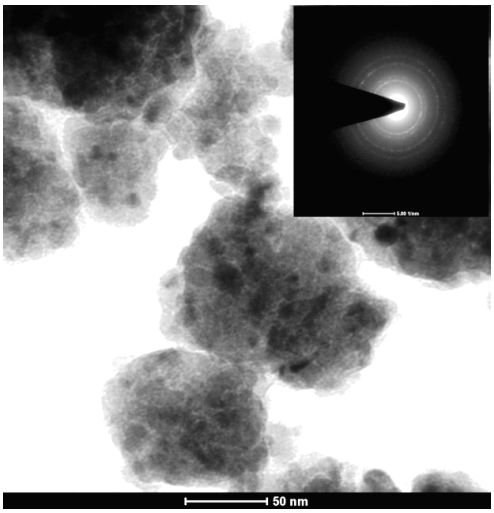

Figure 3

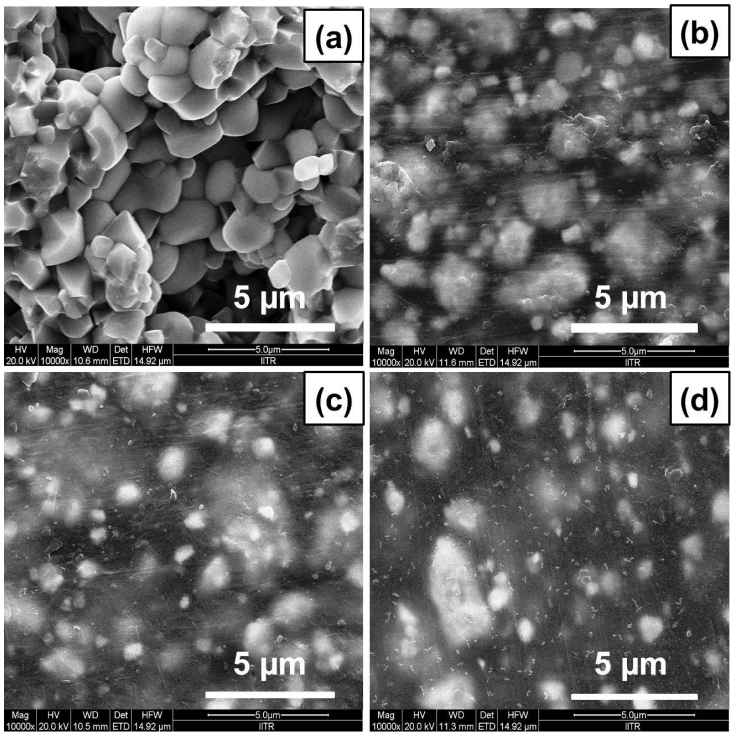

Figure 4

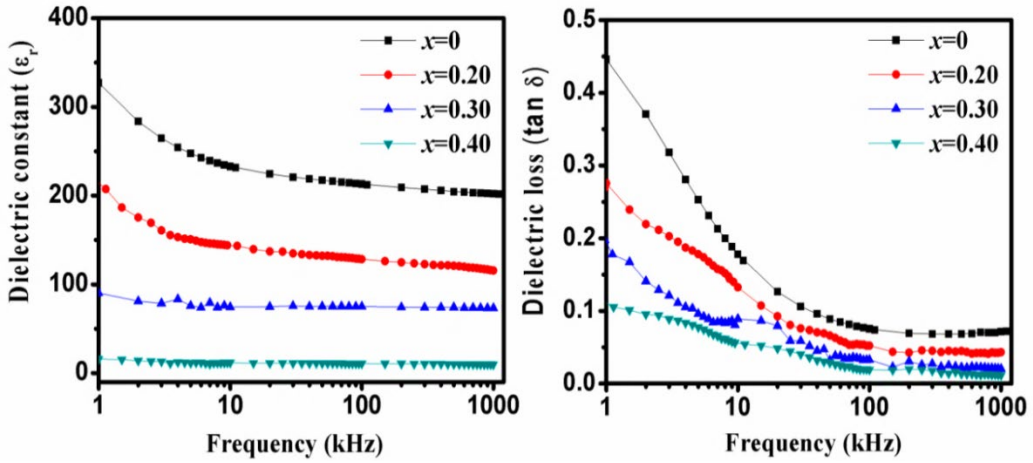
Dielectric constant (ε_r)
Frequency (kHz)
x=0
x=0.20
x=0.30
x=0.40
Dielectric loss (tan δ)
Frequency (kHz)
x=0
x=0.20
x=0.30
x=0.40

Figure 5

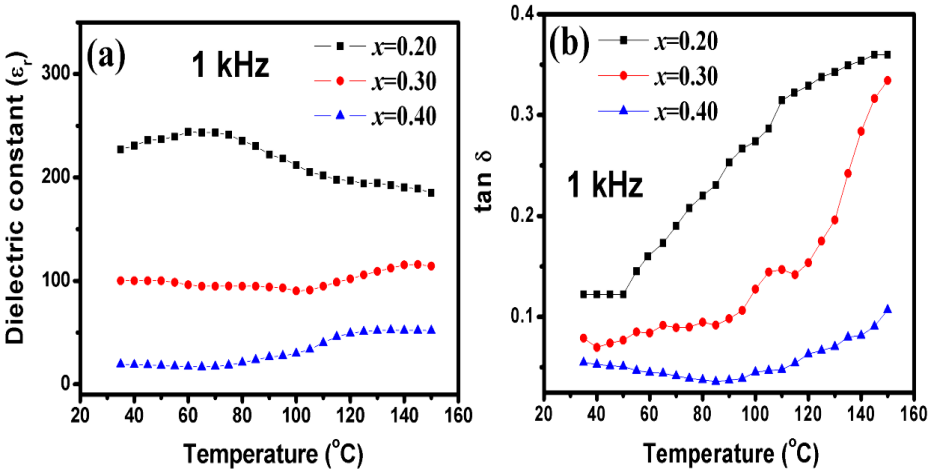
(a)
1 kHz
x=0.20
x=0.30
x=0.40
Dielectric constant (ε_r)
Temperature (°C)
(b)
1 kHz
tan δ
Temperature (°C)

Figure 6

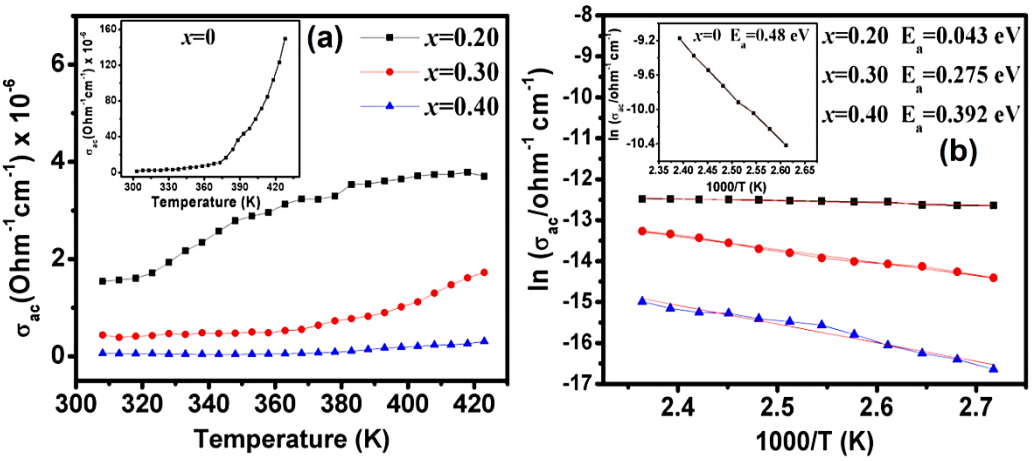
(a)
x=0
x=0.20
x=0.30
x=0.40
Temperature (K)
(b)
x=0 Ea=0.48 eV
x=0.20 Ea=0.043 eV
x=0.30 Ea=0.275 eV
x=0.40 Ea=0.392 eV
1000/T (K)

Figure 7

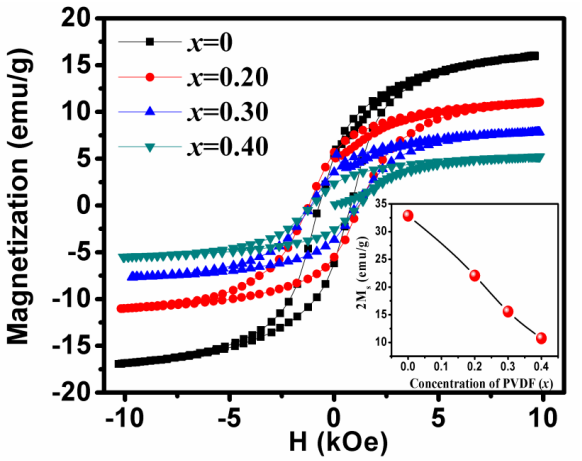
x=0
x=0.20
x=0.30
x=0.40
Magnetization (emu/g)
H (kOe)
2M_s (emu/g)
Concentration of PVDF (x)

Figure 8

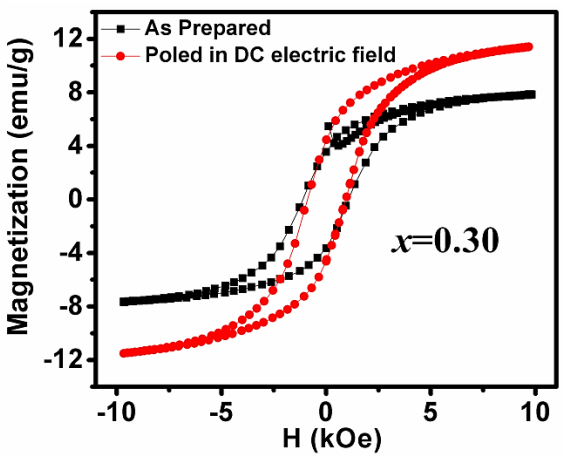
As Prepared
Poled in DC electric field
Magnetization (emu/g)
12
8
4
0
-4
-8
-12
-10
-5
0
5
10
H (kOe)
x=0.30

Figure 9

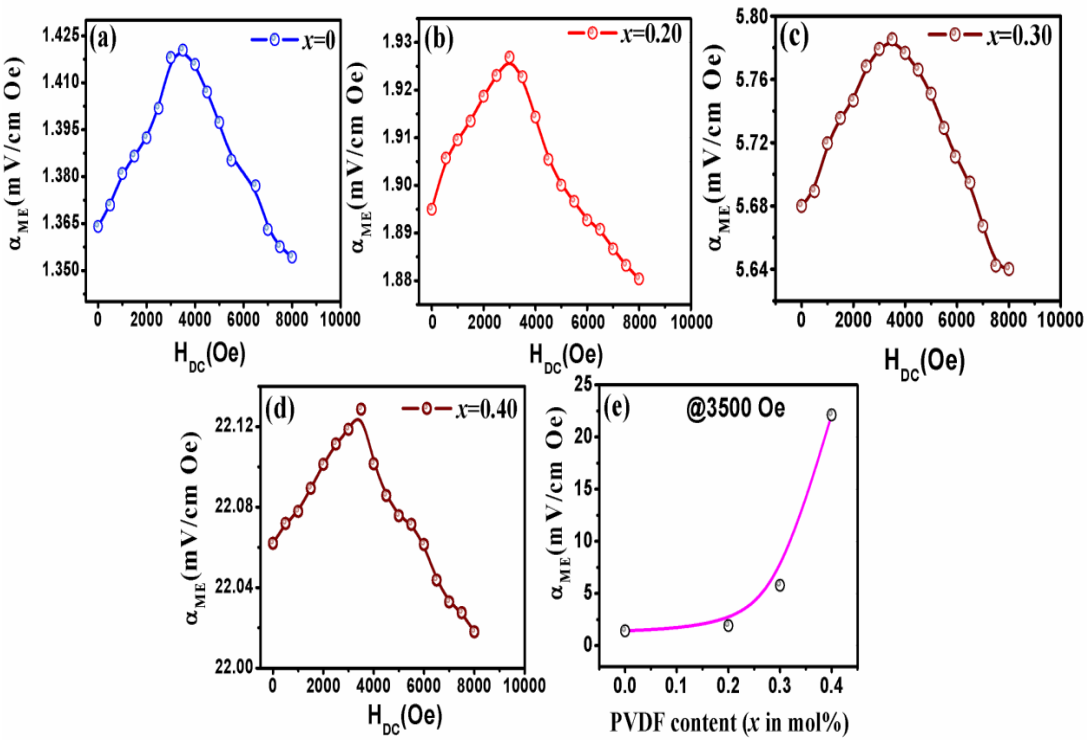
(a)
x=0
(b)
x=0.20
(c)
x=0.30
(d)
x=0.40
(e)
@3500 Oe
α_ME (mV/cm Oe)
H_DC (Oe)
PVDF content (x in mol%)

Figure 10

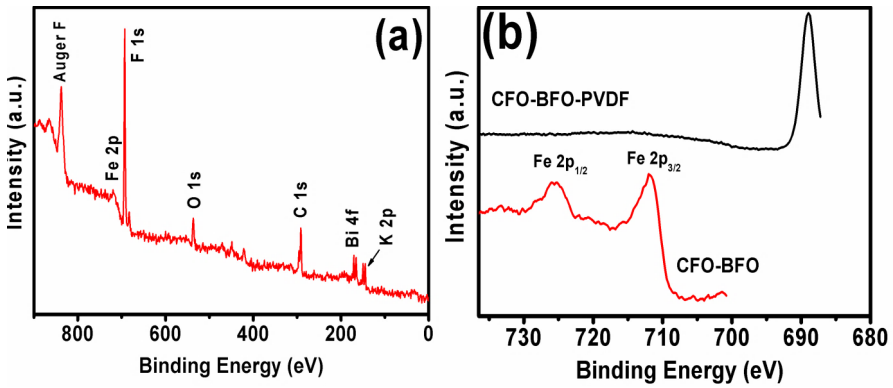
(a)
Auger F
F 1s
Fe 2p
O 1s
C 1s
Bi 4f
K 2p
Intensity (a.u.)
800
600
400
200
0
Binding Energy (eV)
(b)
CFO-BFO-PVDF
Fe 2p1/2
Fe 2p3/2
CFO-BFO
Intensity (a.u.)
730
720
710
700
690
680
Binding Energy (eV)

Figure 11